Acta Materialia 120 (2016) 168–178

Contents lists available at ScienceDirect

Acta Materialia

journal homepage: www.elsevier.com/locate/actamat

Full length article

Grain refinement of hypoeutectic Al-Si alloys with B

Zongning Chen [a, b], Huijun Kang [a, c], Guohua Fan [d], Jiehua Li [e], Yiping Lu [a], Jinchuan Jie [a], Yubo Zhang [a], Tingju Li [a], Xigao Jian [b], Tongmin Wang [a, *]

[a] Key Laboratory of Solidification Control and Digital Preparation Technology, School of Materials Science and Engineering, Dalian University of Technology, Dalian 116024, PR China
[b] School of Chemical Engineering, Dalian University of Technology, Dalian 116024, PR China
[c] Laboratory of Special Processing of Raw Materials, Dalian University of Technology, Dalian 116024, PR China
[d] School of Materials Science and Engineering, Harbin Institute of Technology, Harbin 150001, PR China
[e] Institute of Casting Research, Montanuniversität Leoben, Leoben A-8700, Austria

ARTICLE INFO

Article history:
Received 13 May 2016
Received in revised form
13 August 2016
Accepted 16 August 2016
Available online 29 August 2016

Keywords:
Grain refinement
Al-Si alloys
Nucleation
Edge-to-edge matching model

ABSTRACT

The enhanced grain refining efficiency of B in treating hypoeutectic Al-Si alloys has been identified for more than 30 years. However, its exact underlying mechanism remains to be explored. Here, we report that AlB_2 could be a highly efficient nucleating substrate for α-Al in Al-Si alloys with high Si concentrations. The addition of AlB_2 alone without the presence of Si does not result in a significant grain refinement. The enhanced grain refining efficiency can be mainly attributed to the enhanced heterogeneous nucleation of AlB_2 caused by Si. It is proposed that the creation of a layer of SiB_6 at the interface between AlB_2 and Al may reduce the crystallographic mismatch, which can significantly improve the nucleating potency of AlB_2. Furthermore, the formation of SiB_6 layer may occur for only a limited span of time in Al-Si melt, and it may further transform to other stable phase (e.g. Si). This investigation reveals the nucleating behavior of AlB_2 influenced by solute Si and thereby sheds some novel insights on the grain refinement mechanism of Al alloy.

1. Introduction

For more than half a century, the grain refinement of Al alloys through inoculation (e.g. Al-Ti-B) has been widely investigated not only for elucidating the grain refinement mechanism but also for developing novel grain refiners [1–4]. Various mechanisms were proposed to interpret the different efficiency of different grain refiners. Generally, two factors are believed to play important roles in grain refinement. One factor is the heterogeneous nucleation. An enhanced heterogeneous nucleation is believed to be responsible for an enhanced grain refinement of Al alloy. The other factor is the growth restriction factor (Q) caused by constitutional undercooling. According to Johnsson's study [5], it is well-accepted that, besides nucleating particles, the role of solutes is also crucial for the grain refinement of Al alloy [6–13]. This theory takes into account the solute elements by observing their effects on Q. It should be noted here that Q is often used to quantify the effects of a solute on grain refinement by the following Equation (1), as originally derived by Maxwell and Hellawell [14]:

$$Q = C_0 m(k-1) \tag{1}$$

where C_0 is the initial solute concentration, m is the liquidus slope, and k is the equilibrium partition coefficient of the alloy. Maxwell and Hellawell [14] made a seminal contribution to developing a predictive model for grain size. The basis of their model is that the growth restriction of already nucleated grains permits further nucleation in the undercooled melt. Furthermore, Greer et al. [15] proposed a free growth model, which correlates the critical undercooling necessary for the free growth with the particle geometry. The free growth model can be, therefore, used to quantitatively describe the grain refining efficiency in terms of the size and size distribution of nucleants. Following the precedent success of the free growth model, many numerical approaches [16–18] and analytical models [19–23] have been developed to predict the as-cast grain size by relating Q to the grain refining efficiency of an inoculant. One example with a good approximation is the simple linear relationship between average grain size, l, and $1/Q$, as suggested by Easton and StJohn [6,12,24]:

* Corresponding author. School of Materials Science and Engineering, Dalian University of Technology, No. 2 Linggong Road, Dalian, Liaoning, PR China.
E-mail address: tmwang@dlut.edu.cn (T. Wang).

http://dx.doi.org/10.1016/j.actamat.2016.08.045
1359-6454/

$$l = a + b/Q \quad (2)$$

where a and b are empirical constants and are related to the number density of active nucleating particles and the efficiency of the nucleating particles, respectively.

It is worth noting that the above-mentioned models were mainly developed to interpret the grain refinement of wrought grades Al alloys by Al-Ti-B grain refiner. For the foundry alloys, in particular to the Al-Si alloys with high Si concentrations, the grain refinement performance of Al-Ti-B grain refiner is less efficient. The so-called Si poisoning occurs when Si concentrations are higher than 3.5 wt% [6,25–32]. To reduce or avoid the Si poisoning, one effective way is to introduce B into the Al-Si system. This operation is often achieved by adding Al-B master alloy, in which AlB_2 resides as the source to supply B, into the melt. The use of Al-B master alloys for the grain refinement of Al–Si alloys was first reported by Wu et al. dating back to 1980s [33]. When Al-B master alloys are used as the refiner, the grain size is continually reduced even with increasing Si content [32]. Since AlB_2 is the dominated particulate phase in Al-B master alloys, it is reasonable to expect that AlB_2 should be a potent nucleating substrate for α-Al [34–36]. But a number of observations [34,37–41] have also shown that AlB_2 alone in the absence of Si cannot effectively refine Al, indicating that the solute Si may interfere with AlB_2 to enhance its nucleating potential. There is still a lack of unambiguous understanding of the physical mechanism. The literature has reported a number of investigations [42–49], in which heterogeneous nucleation is strongly dependent on the interfacial structure and composition between nucleant and solid phase. Especially, atomic layering at the solid/substrate interface may significantly affect the nucleating potency of a particle. For example, the formation of a Ti-rich monolayer (Al_3Ti) on the basal plane of TiB_2 particle had been postulated to interpret the grain refinement mechanism of Al-5Ti-1B (wt%) in theoretical [44,46,50] and experimental investigations [43,48,49]. Similarly, in the case of Al-Si alloys refined by B, there may also be an interaction between AlB_2 and Si, which may have a great impact on the heterogeneous nucleation behavior of α-Al, and thereby the grain refinement of the alloy. In the present work, the interfacial structure and composition between AlB_2 and Si are investigated with a special aim to elucidate the effects of Si on the grain refining efficiency of AlB_2.

Apart from experimental evidences, the edge-to-edge matching (E2EM) model has also been well documented to be a powerful tool in predicting possible orientation relationships (OR) between a nucleant substrate and solid phase [51]. The E2EM model was originally proposed by Zhang and Kelly [52,53] to study the interface between precipitates and matrix and then extended to elucidate the nucleation in grain refinement [54,55]. Two parameters are involved in E2EM model. One is the interatomic misfit (f_r) and the other is the interplanar mismatch (f_d). When $f_r < 10\%$ and $f_d < 10\%$, an OR between two phases can be predicted. In the present work, E2EM model will be used to evaluate possible crystallographic changes and then compare with the experimental observations.

2. Experimental

Al-3B master alloy (all compositions are in wt% unless otherwise specified) was synthesized by an improved halide salt reaction method [56]. The microstructure of the master alloy was examined by scanning electron microscopy (SEM) using a Zeiss Supra55. Phase identification was carried out using a PANalytical Empyrean X-ray diffractometer (XRD). A 15% NaOH aqueous solution was used for deep-etching to reveal the three-dimensional (3D) morphology of the AlB_2 particles. The size distribution of the AlB_2 particles was measured by analyzing the SEM micrographs. The total number of AlB_2 particles is in an order of 1000.

Commercial purity (CP) Al (99.8%) and high purity Si (99.97%) were melted in a medium-frequency induction furnace to produce a series of Al-Si alloys with various nominal compositions (1.0, 2.0, 3.0, 4.0, 5.5, 7.0, 8.5 and 10.0% Si) at 780 °C. The melts were transferred to a resistance furnace to perform grain refinement tests with the addition of Al-3B master alloy. A reference sample was taken from each melt to compare the grain structure of the alloy before and after inoculation. The Al-B inoculants were then added into the melts at 720 °C. The B concentration is up to 200 ppm. After stirring, the melt was cast into a preheated graphite mold with an average cooling rate of 1.5 K/s at the center of the casting.

In order to evaluate the effect of the Si enrichment on the refining efficiency of AlB_2 during isothermal holding experiments, a nominal Al-7Si-2B alloy was prepared by the same method as described above. One percent addition of the Al-7Si-2B alloy was then made to CP Al at 720 °C. For comparison, Al-3B master alloy was also added to CP Al. In the two trails, the same Si levels was adjusted by alloying Si in CP Al via the addition of Al-3B master alloy. The melt was cast by the same method as described above to perform the grain refinement tests.

Metallographic samples were sectioned 20 mm above the bottom of the casting. Standard metallographic procedures were carried out to prepare the sections for grain size measurements. The polished samples were anodized in Barker's reagent (1 mL of HBF_4 in 200 mL of distilled water) and then examined with optical microscopy (OM) under a polarized light mode. The images were taken from the same regions. The grain size was measured by the lineal intercept method (ASTM standard E112-10). The reported values are an average of at least 100 measurements.

To investigate the crystallographic orientation relationship (OR) between the AlB_2 and Al matrix, two extra grain refinement trials were performed on Al-2Si and the Al-7Si alloy. In these two trials, the B addition is up to 0.2% (2000 ppm) to improve the detectability of AlB_2 in the Al matrix. The ORs were determined using an automated electron backscatter diffraction (EBSD) facility installed in the SEM. The microstructure of the 0.2%B refined Al-7Si alloy was observed under a Leica MEF-3 optical microscope. The AlB_2 particles at the center of α-Al grains were reproducibly identified by SEM equipped with an energy dispersive X-ray (EDX) spectrometer. A representative AlB_2/Al pair was positioned in the central field of view, and TEM foils containing AlB_2/Al interface were prepared using focused ion beam (FIB, FEI-600i Helios NanoLab) operated at 2.0 kV and 23 pA for the ion beam at the final thinning stage. Transmission electron microscopy (TEM) and scanning transmission electron microscopy (STEM) were conducted in a Tecnai G2-F30 microscope operated at 200 kV. High-resolution TEM (HRTEM) was conducted in a Cs-corrected JEOL-2100F microscope operated at 200 kV.

3. Results

3.1. Microstructure of the Al-B master alloy

Fig. 1a shows the microstructure of the Al-3B master alloy. It is featured by a uniform dispersion of boride particles in Al matrix, being free of residual salt, oxides and other inclusions. The XRD spectrum (Fig. 1b) shows reflections of AlB_2 phase and Al matrix, indicating that the only species to be introduced into the melt are AlB_2 particles. Fig. 1c and d are SEM images showing 3D morphology of the AlB_2 particles in the deep-etched Al-3B master alloy. The AlB_2 particles exhibit well-developed hexagonal block/

plate-like shapes. Particle clusters were occasionally observed (Fig. 1c), but most of the AlB_2 particles are in the form of discrete particulates, exposing their {0001} basal plane and $\{10\bar{1}0\}$ prism plane. Some $\{10\bar{1}1\}$ bevel planes were also observed to link the basal and prism planes. A statistical data analysis of the particle size distribution is shown in Fig. 1e, which can be well fitted by a lognormal function with an average value of 3.1 μm. More than three-quarters of the AlB_2 particles fall in the range of 1–5 μm. According to the free growth model [15], the particles in this range are much more likely to be activated in initiating new grains under typical solidification conditions.

3.2. Grain refinement of Al-Si alloys by Al-B master alloy

The inoculation of the Al-3B alloy was defined to be 0.02% (200 ppm) B, which has been reported to be an optimum for Al-7Si alloy [34,39]. Fig. 2 shows the as-cast grain structures of CP Al and Al-7Si alloy with and without inoculation. The grain structure of CP Al is coarse and predominantly columnar (Fig. 2a). Although the Al-B alloy tends to supply sufficient nucleating particles, the addition of B does not result into a significant change on the grain structure (Fig. 2a and b). This is taken to imply that in the absence of adequate solute, AlB_2 alone is not an effective nucleation site for the grain refinement of Al. In contrast, the inoculation of Al-7Si alloy does result into a significant change on the grain structure (Fig. 2c and d). After adding 200 ppm B, the average grain size of Al-7Si alloy is reduced from 1096 ± 223 μm to 216 ± 70 μm. More importantly, a uniform and equiaxed grain structure was observed. Clearly, an enhanced grain refining efficiency was obtained with the presence of Si.

To further illustrate the effects of Si on the grain refining performance of AlB_2, Fig. 3 shows the measured grain size in a series of Al(-Si) alloys with and without the addition of 0.02% B, as a function of Si contents. The grain size without B addition, shows a "V" type trend with a transition point at ~3% Si. After the transition point, the grain size increases with increasing Si contents. This transition has been reported by other researchers [26,27,30–32], but to date, there is no consensus on its mechanism. Interestingly, with the presence of Si and AlB_2 together, an opposite trend was observed. The grain size continues to decrease with increasing Si contents. The discrepancy in grain refining efficiency of AlB_2 with varying Si was observed to start in the range 4.0–5.5% Si, which is fully consistent with the previous results [32]. Such discrepancy cannot be explained simply by growth restriction of Si because other solutes (e.g., Zn, Mg, Cu, etc.) with similar Q values do not provide a comparable efficacy with respect to Si [57].

Fig. 4 shows the measured grain size in the literature [32,34,58,59] and in the present work, versus 1/Q and the fitted lines predicted by Eq. (2). When the Si concentration is less than or close to 4.0 wt%, the experimental data can be well fitted by $l = a + b/Q$, with $a = 320$ and $b = 1500$, whereas at higher Si concentrations (>5.5 wt%), a good agreement is obtained with $a = 10$ and $b = 8500$. Since the value a is related to the number density of active nucleating particles, a smaller a means that more particles can be activated as nucleants. It is, therefore, reasonable to infer that an enhanced nucleation of α-Al on AlB_2 may occur at higher Si concentrations. All results strongly indicate that the presence of Si is necessary to activate the refining efficiency of AlB_2.

3.3. Refining efficiency of AlB_2 during isothermal holding

Fig. 5 shows the grain refinement performance tests of the experimental Al-3B and an Al-7Si-2B alloy at an addition level of 200 ppm B during isothermal holding. A significant grain refinement was obtained in CP Al by adding 200 ppm B via the Al-7Si-2B alloy. The sample after inoculation for 2 min exhibits a fine and equiaxed grain structure, which was somewhat retained for nearly 60 min. However, with prolonged holding, fading of the grain refinement is visible. Nearly complete loss of grain refinement was observed after 240 min of isothermal holding at 720 °C. In contrast,

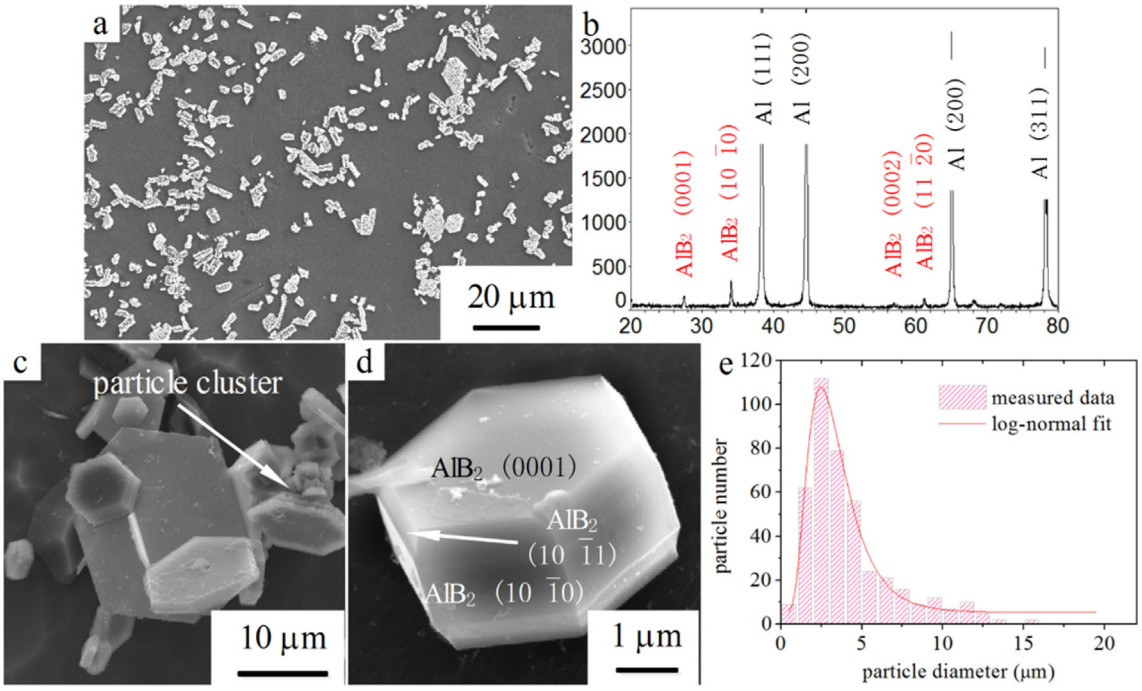

Fig. 1. Characterization of the experimental Al-3B master alloy. (a) SEM micrograph showing the microstructure of the master alloy; (b) XRD spectrum of the alloy; (c) the 3D morphology of typical particle clusters revealed by deep-etching, (c) the 3D morphology of individual boride particles revealed by deep-etching, and (e) the measured size distribution of AlB_2 particles and its corresponding lognormal fitting.

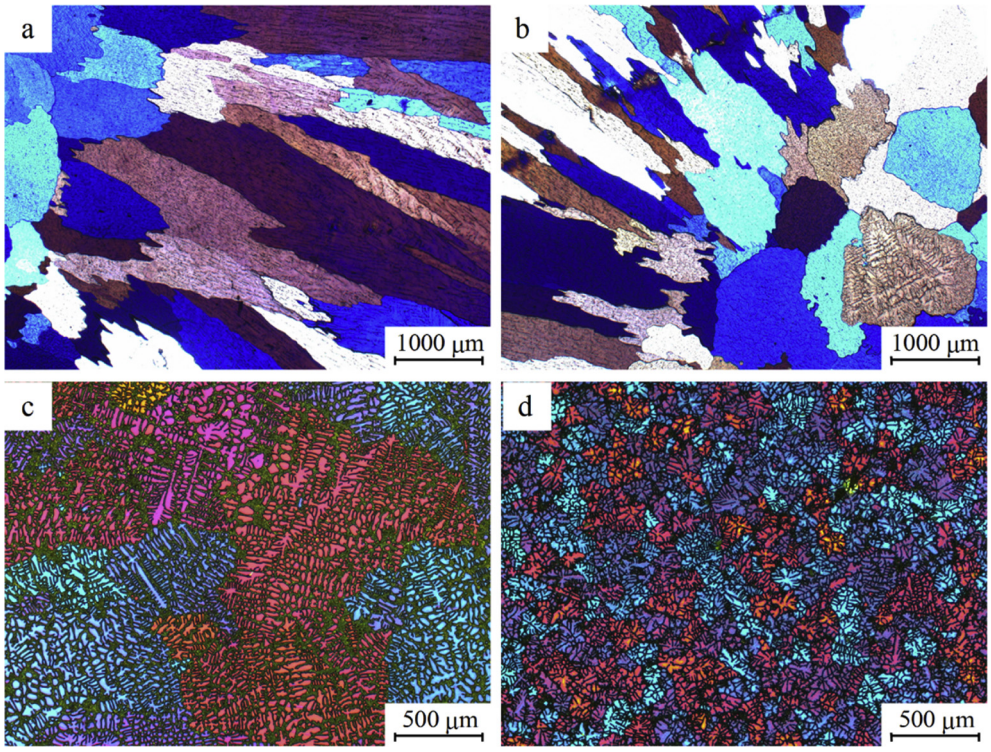

Fig. 2. Grain structure of Al and Al-7Si alloy with/without B inoculation: (a) Al; (b) Al with 200 ppm B; (c) Al-7Si alloy; (d) Al-7Si alloy with 200 ppm B.

no significant grain refinement was observed in the reference experiment, where 200 ppm B was added via Al-B master alloy in spite of the same Si levels.

3.4. ORs between AlB_2 and Al

Fig. 6a and b shows typical SEM micrographs of the overly concentrated (0.2% B) Al-2Si and Al-7Si alloys, respectively. Clearly, some AlB_2 particles were observed within Al grains. The corresponding Kikuchi patterns reflected from the AlB_2 and the Al matrix are presented in Fig. 6c and d for Al-2Si-0.2B and in Fig. 6e and f for Al-7Si-0.2B, respectively. Some indexes are marked on the patterns. No evident ORs can be identified in Al-2Si-0.2B sample. This indicates that these AlB_2 particles may be merely engulfed by the solidification interface front, and are not responsible for the nucleation of Al grains. In the patterns of the Al-7Si-0.2B sample, however, the $(1\bar{1}1)_{Al}$ Kikuchi band is almost parallel to the $(0001)_{AlB2}$ band, while the $[\bar{1}10]_{Al}$ and $[\bar{1}21]_{Al}$ Kikuchi poles are very close to the $[\bar{2}110]_{AlB_2}$ and $[\bar{1}100]_{AlB_2}$ poles, respectively. The OR can be expressed as:

$$\left\{1\bar{1}1\right\}_{Al}//\{0001\}_{AlB_2},\quad <\bar{1}10>_{Al}//<\bar{2}110>_{AlB_2}$$
$$\left(\text{or } <\bar{1}21>_{Al}//<\bar{1}100>_{AlB_2}\right)$$

where the two pairs of direction relationships are identical once the former plane relationship is fixed.

Considering the fact that a direct comparison of the poles and bands in Kikuchi patterns may be less accurate, a statistical method

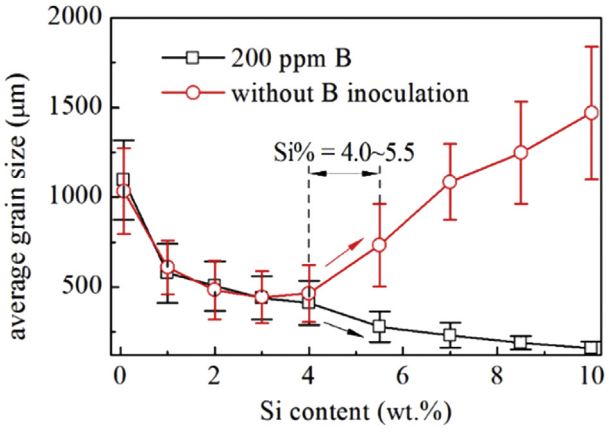

Fig. 3. The average grain size in a series of Al-Si alloys with and without the addition of 200 ppm B.

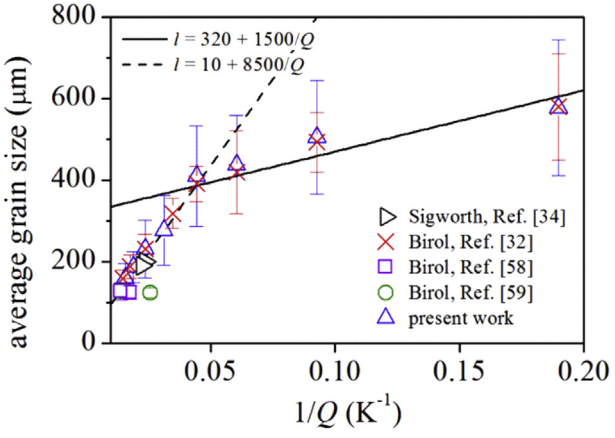

Fig. 4. Comparison of experimentally measured grain size data versus 1/Q with fitting according to Eq. (2) for the Al-Si alloys with 200 ppm B.

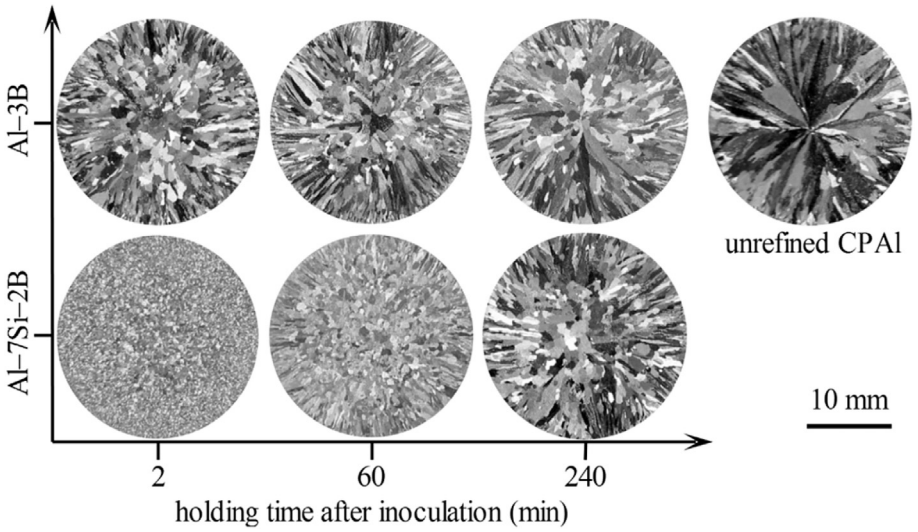

Fig. 5. The grain refinement performance tests in CP Al with the addition of 200 ppm B via Al-3B and Al-7Si-2B alloy during isothermal holding, respectively.

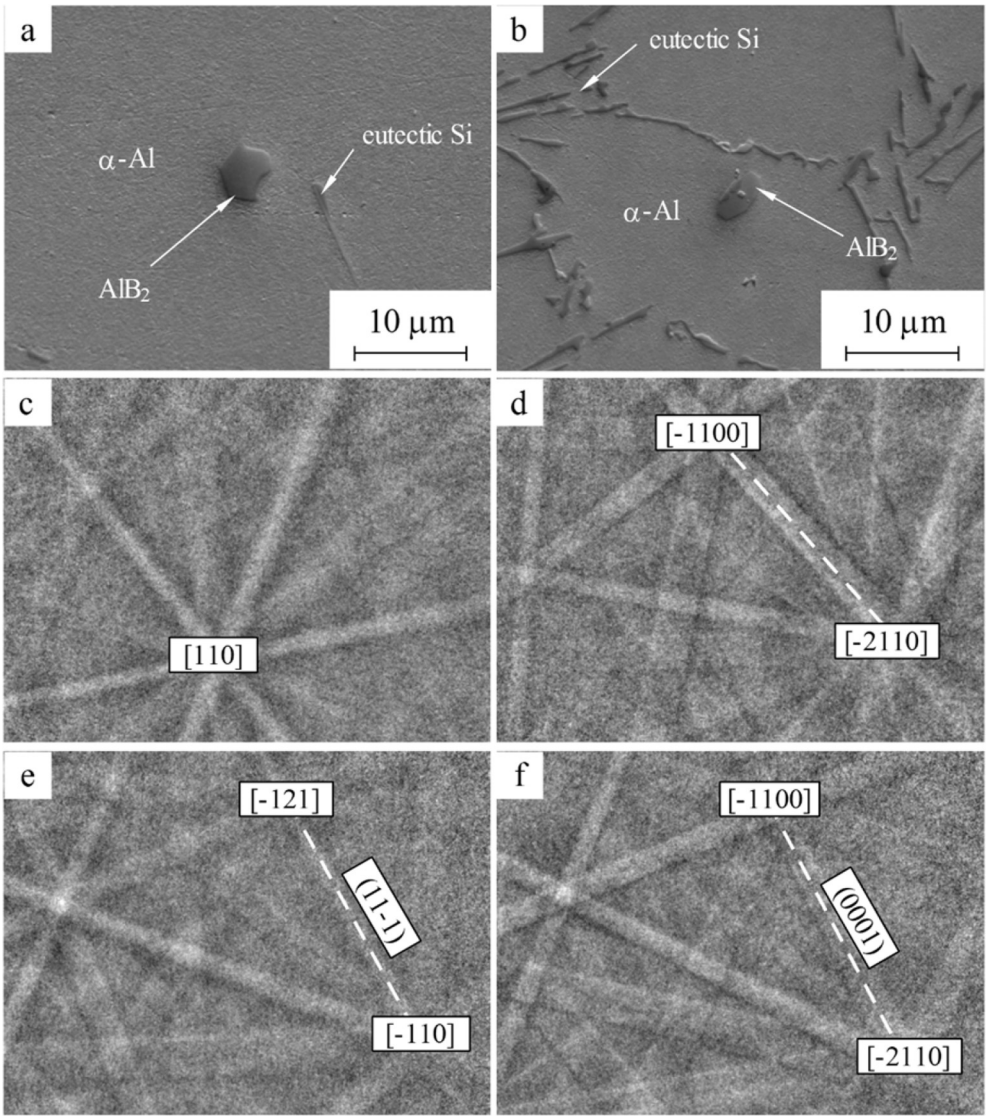

Fig. 6. SEM micrographs of (a) Al-2Si-0.2B and (b) Al-7Si-0.2B samples showing AlB_2 particles within Al matrix. (c)/(d) and (e)/(f) correspond to the Kikuchi patterns of Al/AlB_2 in (a) and (b), respectively.

based on Euler angles [60] was used to confirm the OR between AlB_2 and Al. The reproducible examination of a large number of AlB_2/Al pairs provides a further experimental support more accurately and statistically. Fig. 7a shows the experimentally determined Al poles, which are parallel to the $[\bar{2}110]_{AlB_2}$ and $[\bar{1}100]_{AlB_2}$ poles in the Al-2Si-0.2B sample. Thirty AlB_2/Al pairs were collected. The Euler angles of Al poles in the $(1\bar{1}1)_{Al}$ projection were calculated and presented in an AlB_2 hcp stereographic projection in terms of $(0001)_{AlB2}$. It is very clear that the Euler angles of Al exhibit random distributions, as shown in Fig. 7a. Hence, no distinguishable ORs can be identified. In contrast, two ORs were reproducibly observed in the Al-7Si-0.2B sample (Fig. 7b– d):

$$<\bar{1}10>_{Al}//<\bar{2}110>_{AlB_2} \text{ and } <\bar{1}21>_{Al}//<\bar{1}100>_{AlB_2}$$

from which the plane matching $\{1\bar{1}1\}_{Al}//\{0001\}_{AlB2}$ can be simply derived based on the crystal structures of the two phases.

Another important parameter that can also be determined is the angular deviation between the matching planes and directions. The refined ORs are as follows:

$$<\bar{1}10>_{Al} 1.9 \text{ from } <\bar{2}110>_{AlB_2} \text{ and } <\bar{1}21>_{Al} 1.6 <\bar{1}100>_{AlB_2}$$

3.5. TEM characterization of the ORs between AlB_2 and Al

Fig. 8a shows TEM bright field image of the AlB_2 particle embedded in the Al matrix. The selected area electron diffraction (SAED) patterns are shown in Fig. 8b and c. Clearly, $[110]_{Al}$ is almost parallel to the $[11\bar{2}0]_{AlB_2}$ zone axis, with only a few degrees of deviation. The superimposed SAED pattern (Fig. 8d) with indexing also clearly demonstrates the following OR between the AlB_2 and α-Al:

$$\{002\}_{Al} 3.9 \text{ from } \{\bar{1}101\}_{AlB_2} \text{ and } <110>_{Al} 1.2 \text{ from } <11\bar{2}0>_{AlB_2}$$

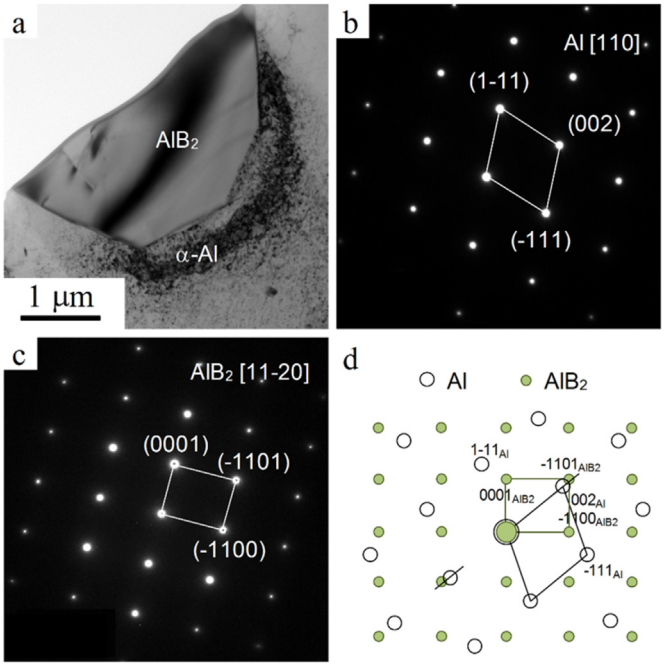

Fig. 8. (a) TEM bright field image of the interface between the AlB_2 and α-Al; (b) SAED pattern of Al with $[110]_{Al}$ zone axis; (c) SAED pattern of AlB_2 with $[11\bar{2}0]_{AlB_2}$ zone axis; and (d) the superimposed spot diffraction patterns showing the OR: $\{002\}_{Al}//\{\bar{1}101\}_{AlB_2}$ and $<110>_{Al}//<11\bar{2}0>_{AlB_2}$.

It should be noted that the OR ($<\bar{1}10>_{Al}//<\bar{2}110>_{AlB_2}$ and $<\bar{1}21>_{Al}//<\bar{1}100>_{AlB_2}$) is based on the lattice parameters of AlB_2 and Al. The angular deviation between the matching planes can be derived: $\{002\}_{Al}$ 3.3° from $\{\bar{1}101\}_{AlB_2}$. The TEM examination is, therefore, in good agreement with the ORs obtained from the EBSD

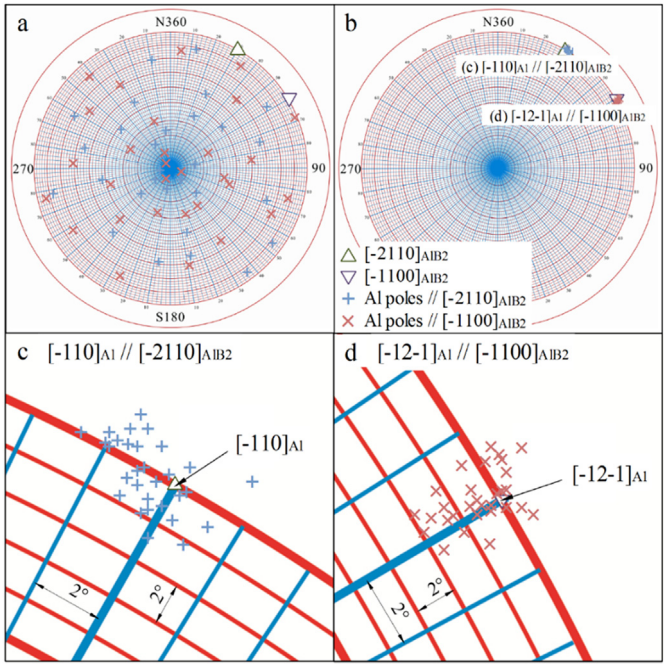

Fig. 7. Stereographic projection with AlB_2 in the (0001) plane, showing the ORs between Al and AlB_2 in (a) Al-2Si-0.2B and (b) Al-7Si-0.2B samples. (c) and (d) are the enlarged portions close to the $[\bar{2}110]_{AlB_2}$ and $[\bar{1}100]_{AlB_2}$ poles in (b).

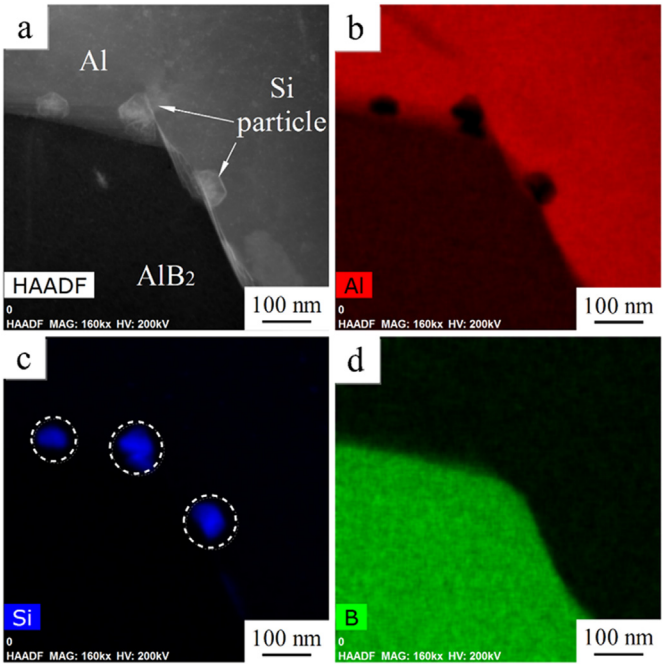

Fig. 9. Microstructure of the interface between AlB_2 and Al matrix: (a) HAADF STEM, and corresponding EDX mappings of (b) Al, (c) Si, and (d) B. The circles in (c) mark the Si particles at the interface.

results. In the terms of crystallographic matching, AlB_2 appears to be an efficient substrate for nucleating α-Al with the presence of high levels of Si.

3.6. STEM and HRTEM characterization of the interface between AlB_2 and Al

Apart from the ORs between AlB_2 and α-Al, Si particles were also observed in the vicinity of AlB_2 particle. Fig. 9a shows the high angle annular dark field (HAADF) STEM micrograph of the same FIB sample showing three strong spots with a bright contrast embedded in the Al matrix occurring at the AlB_2/Al interface. Contrast in HAADF STEM image scales to a good approximation with the atomic number Z of the observed material as ~ $Z^{1.7}$ so that columns containing Si atoms within the Al matrix are clearly distinguishable with a brighter intensity, an observation also clearly confirmed by the chemical maps obtained with EDX maps, as shown in Fig. 9b–d.

Fig. 10 shows TEM bright field images (Fig. 10a and d) and HRTEM images (Fig. 10b and e) of one Si particle in the vicinity of AlB_2 particle. When the AlB_2 particle is tilted to $[01\bar{1}0]_{AlB_2}$ zone axis (Fig. 10c, fast Fourier transform (FFT)), no crystallographic matching was observed between the AlB_2 particles and Si particle. Similarly, when the Si particle is tilted to $[\bar{1}12]_{Si}$ zone axis (Fig. 10f, FFT), no crystallographic matching was detected. This indicates that AlB_2 appears to be not an efficient nucleation substrate for Si.

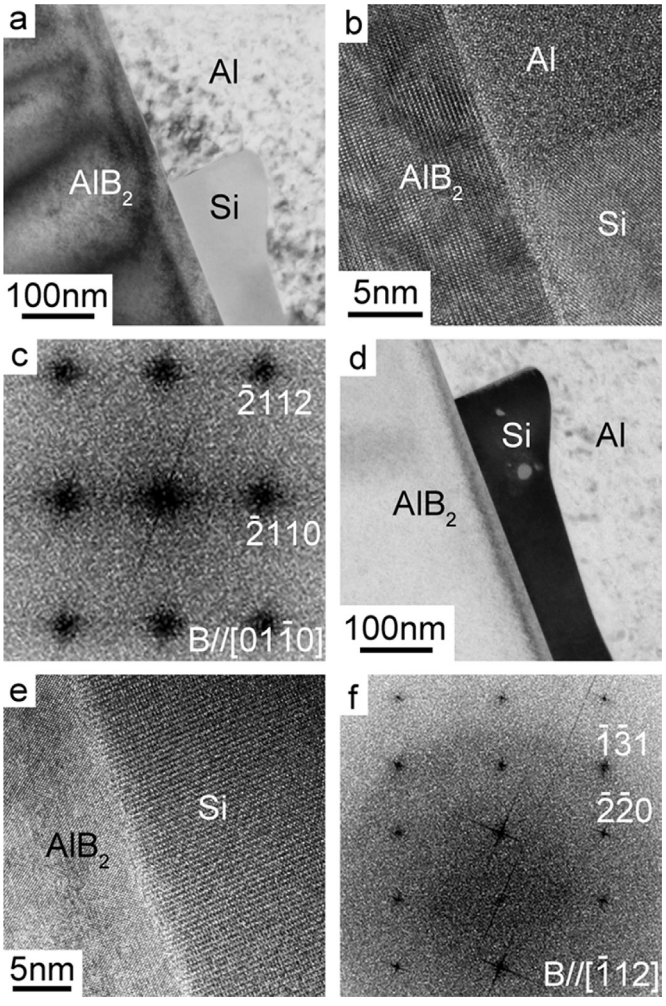

Fig. 10. (a) TEM bright field image of the interface between the AlB_2 and Si; (b) HRTEM image of Al the interface between the AlB_2 and Si with $[01\bar{1}0]_{AlB_2}$ zone axis; (c) *FFT* of AlB_2 with $[01\bar{1}0]_{AlB_2}$ zone axis; and (d) TEM bright field image of the interface between the AlB_2 and Si; (e) HRTEM image of Al the interface between the AlB_2 and Si with $[\bar{1}12]_{Si}$ zone axis; (f) *FFT* of Si with $[\bar{1}12]_{Si}$ zone axis.

4. Discussion

AlB_2 alone without sufficient Si does not nucleate Al efficiently. Instead, the addition of AlB_2 together with Si indeed enhances the grain refining efficiency. This enhancement in grain refining efficiency caused by Si can be due to twofold: (i) enhanced heterogeneous nucleation of AlB_2, and (ii) increased *Q*, which will be discussed as follows:

4.1. Enhanced heterogeneous nucleation on AlB_2 caused by Si

The Si particle was observed in the vicinity of the AlB_2 particle, as shown in Figs. 9 and 10, may be related to the enhanced grain refining efficiency. When AlB_2 is introduced into molten Al-Si alloys, Si may diffuse to the AlB_2 surface and form some intermetallic compounds coating the substrate. The Si particle could be transformed from other metastable Si-enriched phases, or in this case it could be an absorbed layer or epitaxial growth intermediate layer that bears the same crystal structures with such phases. The intermediate layers are expected to increase the nucleation potency of AlB_2 if their incorporation can reduce the crystallographic mismatch between the substrate and the solid.

To elucidate which type of Si-enriched structures is more likely to form at the interface, E2EM analyses were employed. According to the phase diagram [61], when 0.02% B is bonded in AlB_2, the boride particles are expected to be unstable in Al melt. Vinod Kumar et al. [62] demonstrated that complete dissolution of AlB_2 will take no less than 60 min. Sigworth and Guzowski's grain refinement test results [34] on Al-7Si implied that within the first 5 min of contact time, dissolution of AlB_2 could be negligible. According to the Al-Si-B equilibria diagram in Ref. [63], no ternary phases have been reported, as a result one would have to consult with binary Si-B phase diagram for such phases. There are three possible silicon borides, i.e. SiB_3, SiB_6, and SiB_n, in terms of the thermodynamic equilibria of the binary Si-B system [64]. The crystal structures of these Si-B binary compounds are listed in Table 1. A survey of the lattice parameters suggests that SiB_6 and Al are most likely to form cube-cube OR because SiB_6 has a primitive cubic structure with $a = 0.4142$ nm, which is very close to that of Al ($a = 0.4094$ nm). For clarity, Fig. 11a shows the crystal structure of SiB_6. Each unit cell of SiB_6 bears one Si atom and six B atoms. There are two closed-packed (cp) or nearly cp planes for SiB_6: {100}SiB_6 and {110}SiB_6, which contain cp rows <110>SiB_6 and <100>SiB_6 as possible matching directions, respectively.

The crystallography of AlB_2 with Al has been extensively investigated by Zhang et al. The following ORs has been predicted [54]:

Table 1
The crystal structures of the Si-B binary compounds.

Compound	Structure	Lattice parameters (nm)			JCPDS#
		a	*b*	*c*	
SiB_3	Tetragonal	0.6319	–	1.2713	74–2255 [a]
SiB_6	Cubic	0.4142	–	–	72–1994
SiB_n	Tetragonal	1.113/1.1097	–	2.383/2.388	18-0253/52-1006[b]

[a] The exact formula in JCPDS is $Si_{11}B_{31}$.
[b] SiB_n is isotypic with B-rich solid solution, here the JCPDS numbers 18-0253 and 52-1006 correspond to SiB_{14} and SiB_{18}, respectively.

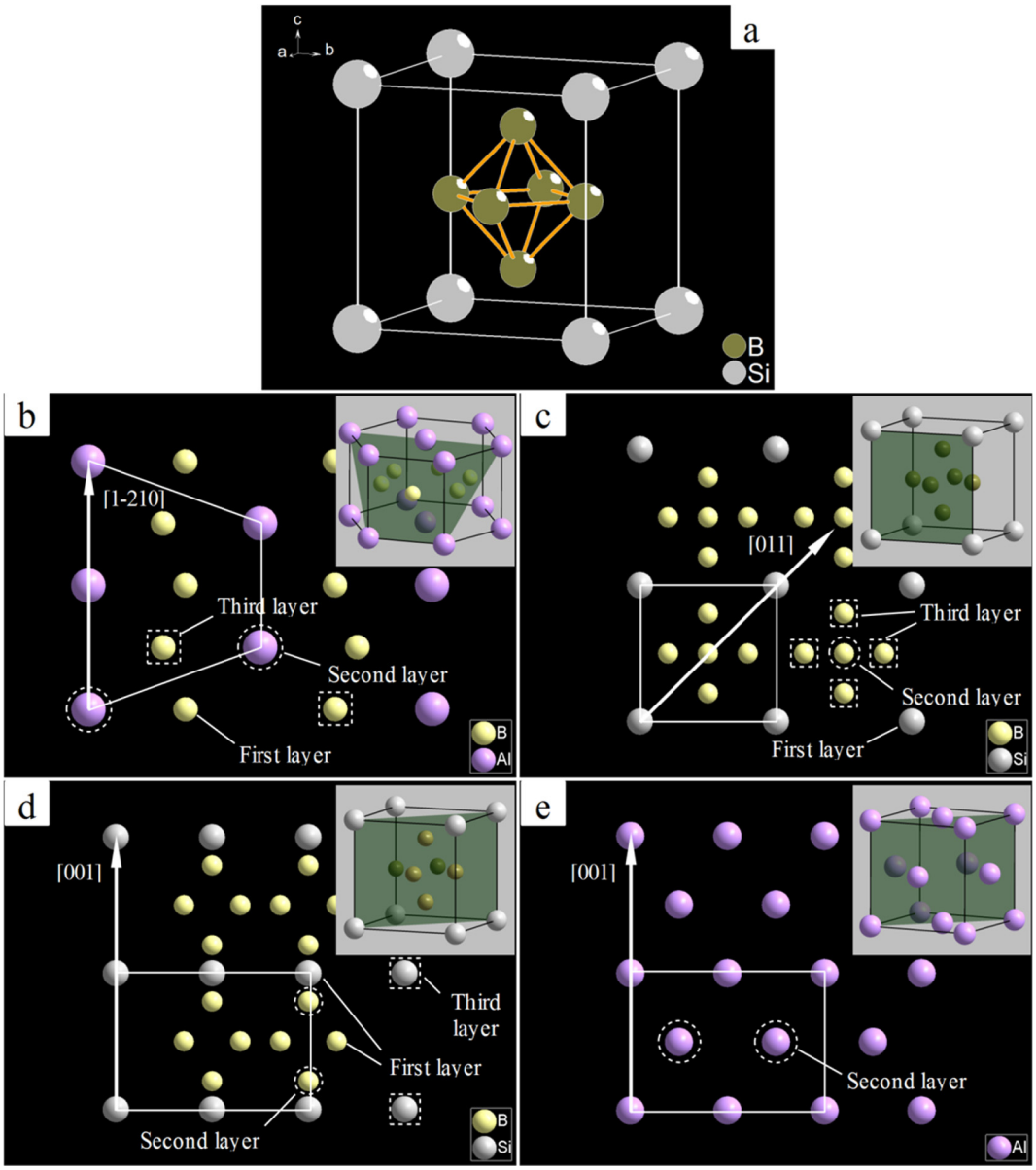

Fig. 11. (a) The crystal structure of SiB_6 and atomic configurations of several cp planes for AlB_2, SiB_6 and Al: (b) $(10\bar{1}1)_{AlB_2}$, (c) $(100)SiB_6$, (d) $(110)SiB_6$, (e) $(220)_{Al}$. The bold solid arrows highlight the cp rows within the planes.

$$\text{OR1: } \{200\}_{Al}//\left\{10\bar{1}1\right\}_{AlB_2} \text{ and } <011>_{Al}//<1\bar{2}10>_{AlB_2};$$

$$\text{OR2: } \{220\}_{Al}//\left\{11\bar{2}0\right\}_{AlB_2} \text{ and } <\bar{1}12>_{Al}//<1\bar{1}00>_{AlB_2}$$

According to the crystallographic data of AlB_2, Al and SiB_6, the f_r and f_d values between specified matching rows and directions can be calculated using the E2EM model. In terms of the criterion $f_r < 10\%$ and $f_d < 10\%$, the following OR group was identified:

$$SiB_6/AlB_2: \{100\}_{SiB_6}//\left\{10\bar{1}1\right\}_{AlB_2} \text{ and } <011>_{SiB_6}//<1\bar{2}10>_{AlB_2};$$

$$Al/SiB_6: \{220\}_{Al}//\{110\}_{SiB_6} \text{ and } <100>_{Al}//<100>_{SiB_6}$$

Fig. 11b and d shows the atomic configuration within the planes listed in the OR group. Bold arrows indicate cp atomic rows on each plane. According to the E2EM model, the cp rows must lie in the matching planes. A possible phase transformation at the interface can be predicted by analyzing the f_r and f_d values of a given OR.

Fig. 12 shows the quantitative data of the two parameters generated from the ORs previously reported by Zhang et al. [54] with the new ORs considering the formation of SiB_6. Forming a layer of SiB_6 among the Al/AlB_2 pair indeed significantly decreases the interatomic mismatch. The f_r values along the $<011>_{Al}//<1\bar{2}10>_{AlB_2}$ and $<\bar{1}12>_{Al}//<1\bar{1}00>_{AlB_2}$ directions both reach 5.1%, whereas those along $<011>SiB_6//<1\bar{2}10>_{AlB_2}$ and $<100>_{Al}//<100>SiB_6$ are 2.7 and 2.2%, respectively. Similarly, calculations of the interplanar mismatch show that the f_d value between matching planes in OR2 has been reduced from 5.1% to 1.7 and 2.3%, which corresponds to the f_d values of $\{100\}SiB_6//\{10\bar{1}1\}_{AlB_2}$ and $\{220\}_{Al}//\{110\}SiB_6$ in the new ORs, respectively. However, compared with the f_d between $\{200\}_{Al}$ and $\{10\bar{1}1\}_{AlB_2}$ in OR1 (0.6%), the newly

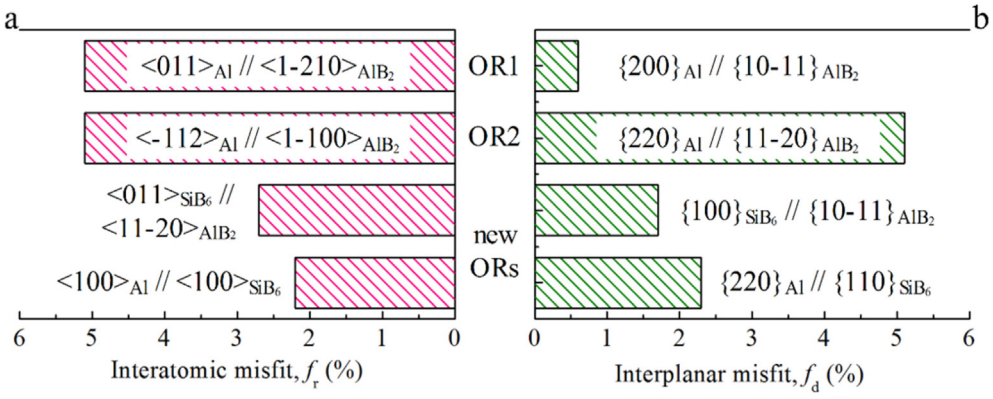

Fig. 12. A comparison of (a) f_r values along the cp rows and (b) f_d values between the cp planes in the OR1 and OR2 for Al/AlB_2 pair, and in the new ORs for Al/SiB_6/AlB_2 group.

formed Al/SiB_6/AlB_2 group increases the f_d. Smaller f_d values tend to alleviate the deviation of matching planes from each other. As reported in Ref. [54], when f_d is equal to or smaller than 6%, the matching planes will be parallel or nearly parallel. In the present case, the f_d values of {100}SiB_6//$\{10\bar{1}1\}_{AlB_2}$ and $\{220\}_{Al}$//{110}SiB_6 are well below 6%, and hence the matching planes should have negligibly small rotations about the matching directions. Furthermore, as indicated in Ref. [65], the f_r value is the dominant factor to determine whether a particle can serve as a potent heterogeneous substrate or not. This indicates that an energetically favorable OR could be established by forming a layer of SiB_6 at the interface between AlB_2 and Al. In contrast, the cp planes of SiB_3 and SiB_n (taking SiB_{14} for instance) are {021}, {104} and {104}, {015}, {006}, respectively, corresponding to $d = 0.2683$, 0.2753 and 0.506, 0.427, 0.398 nm, respectively. A comparison of these values with the interplanar spacings of AlB_2 and Al strongly suggested that SiB_3 and SiB_n cannot form the corresponding ORs as measured by the EBSD and TEM. Therefore, from the E2EM analyses, the enhanced nucleation could be ascribed to the formation of a SiB_6 intermediate layer on AlB_2.

The SiB_6 layer thus formed at the interface between AlB_2 and Al may be not stable upon solidification and further transform to other stable phases (e.g. Si). This suggestion can be evidenced by our isothermal holding experiments. A complete loss of grain refinement was observed after 240 min holding at 720 °C, as shown in Fig. 3, which can be mainly attributed to the dissolution of unstable Si-enriched structure (e.g. SiB_6) on AlB_2 in dilute Al-Si melts. It should be noted here that, the formation of Si-enriched structure is predicted to be favorable according to E2EM model and supported by our isothermal holding experiments, however, the precise identity of the Si-enriched structure (e.g. SiB_6) is still not fully revealed in the present work. Given the fact that the formation of such Si-enriched structures may occur for only a limited span of time, further atomic scale in-situ characterization is required to elucidate the presence of Si-enriched structure and the role it plays during heterogeneous nucleation of Al alloy.

4.2. Increased Q caused by Si

Another important factor that should also be taken into consideration is the increased Q (constitutional undercooling contribution) caused by Si because it is also one of the two essentials for an effective grain refinement. By describing the relationship between grain size and the alloy composition, the linear relationship (Eq. (2)), as presented in Fig. 4, can be used to assess the overall effect of Si on the grain refining efficiency of the Al-Si/AlB_2 system. While as stated earlier, the sudden change in a indicates that, in the range 4–5.5 wt% Si, there exists an increase in the number density of nucleating particles in the Al-Si/AlB_2 system, which is probably attributable to the positive effects of Si on the nucleation potency of AlB_2 by way of modifying the crystallographic mismatch at the interface. The steeper slope (larger value b) of the dotted line in Fig. 4 also implies that the solute may have a more pronounced impact on the growth restriction of α-Al in concentrated Al-Si alloys. However, it should be noted that the effect of Si on growth restriction of α-Al is relatively low. The growth suppression effect of Si on α-Al may be less dominant compared with its effect on the enhancement of heterogeneous nucleation potency of AlB_2.

5. Conclusions

(1) AlB_2 particles are potential nucleating sites for α-Al in Al-Si alloys with high Si concentrations. The potency of AlB_2 particles requires to be activated by the presence of Si with high concentrations.
(2) A transition of grain refining efficiency occurs in the range of 4.0–5.5 wt% Si, above which adding AlB_2 will significantly refine the grain structure of Al-Si alloys.
(3) With the presence of sufficient Si, a reproducible OR between AlB_2 and Al has been identified: $\{1\bar{1}1\}_{Al}//\{0001\}_{AlB2}$, $<\bar{1}10>_{Al}//<\bar{2}110>_{AlB_2}$ (or $<\bar{1}21>_{Al}//<\bar{1}100>_{AlB_2}$). Furthermore, a new set of ORs was predicted using E2EM model for the Al/SiB_6/AlB_2 group: {100}SiB_6//$\{10\bar{1}1\}_{AlB_2}$ and <011>SiB_6//$<1\bar{2}10>_{AlB_2}$; $\{220\}_{Al}$//{110}SiB_6 and $<100>_{Al}$// <100>SiB_6.
(4) The formation of a layer of SiB_6 at the interface between AlB_2 and Al may occur for only a limited span of time. The nucleating potency of AlB_2 can be significantly enhanced by forming a layer of SiB_6 on the exposed surfaces of AlB_2. However, the SiB_6 at the interface between AlB_2 and Al may be not stable in Al-Si melting and further transform to Si particles.

Acknowledgments

The authors gratefully acknowledge the support of the National Natural Science Foundation of China (Nos. 51601028, 51525401, 51274054, 51401044, U1332115) and the China Postdoctoral Science Foundation (2015M581331). The author (T.M. Wang) acknowledges the financial support from Dalian Support Plan for Innovation of High-level Talents (Top and Leading Talents, 2015R013). The author (J.H. Li) acknowledges the access to TEM

instruments at the Erich Schmidt Institute of Materials Science of the Austrian Academy of Science and the financial support from the Major International (Regional) Joint Research Project (No. 51420105005) from China. The authors would like to thank Dr. Yun Wang, Brunel University for his valuable comments on the manuscript and Mr. Chunyong Wu for his help in preparing the anodized metallographic samples.

References

[1] D.G. McCartney, Grain refining of aluminum and its alloys using inoculants, Int. Mater. Rev. 34 (1989) 247–260.
[2] B.S. Murty, S.A. Kori, M. Chakraborty, Grain refinement of aluminium and its alloys by heterogeneous nucleation and alloying, Int. Mater. Rev. 47 (2002) 3–29.
[3] T.E. Quested, Understanding mechanisms of grain refinement of aluminium alloys by inoculation, Mater. Sci. Technol. 20 (2004) 1357–1369.
[4] F. Wang, Z. Liu, D. Qiu, J.A. Taylor, M.A. Easton, M.-X. Zhang, Revisiting the role of peritectics in grain refinement of Al alloys, Acta Mater. 61 (2013) 360–370.
[5] M. Johnsson, A Critical Survey of the Grain Refining Mechanisms of Aluminium, in, Stockholm University, Stockholm, 1993.
[6] M. Johnsson, Influence of Si and Fe on the grain-refinement of aluminum, Z. Fur Met. 85 (1994) 781–785.
[7] M. Johnsson, Influence of Zr on the grain-refinement of aluminum, Z. Fur Met. 85 (1994) 786–789.
[8] M. Johnsson, L. Backerud, The influence of composition on equiaxed crystal growth mechanisms and grain size in Al alloys, Z. Fur Met. 87 (1996) 216–220.
[9] J.A. Spittle, S. Sadli, Effect of alloy variables on grain refinement of binary aluminum-alloys with Al-Ti-B, Mater. Sci. Technol. 11 (1995) 533–537.
[10] M.A. Easton, D.H. StJohn, Grain refinement of aluminum alloys Part I. The nucleant and solute paradigms—a review of the literature, Metall. Mater. Trans. Phys. Metall. Mater. Sci. 30 (1999) 1613–1623.
[11] M.A. Easton, D.H. StJohn, Grain refinement of aluminum alloys Part II. Confirmation of and a mechanism for the solute paradigm, Metall. Mater. Trans. Phys. Metall. Mater. Sci. 30 (1999) 1626–1633.
[12] M.A. Easton, D.H. StJohn, The effect of alloy content on the grain refinement of aluminium alloys, in: J.L. Anjier (Ed.), Light Metals 2001, Minerals, Metals & Materials Soc, Warrendale, 2001, pp. 927–933.
[13] F. Wang, D. Qiu, Z.-L. Liu, J.A. Taylor, M.A. Easton, M.-X. Zhang, The grain refinement mechanism of cast aluminium by zirconium, Acta Mater. 61 (2013) 5636–5645.
[14] I. Maxwell, A. Hellawell, Simple model for grain refinement during solidification, Acta Metall. 23 (1975) 229–237.
[15] A.L. Greer, A.M. Bunn, A. Tronche, P.V. Evans, D.J. Bristow, Modelling of inoculation of metallic melts application to grain refinement of aluminium by Al–Ti–B, Acta Mater. 48 (2000) 2823–2835.
[16] T. Quested, A. Greer, Grain refinement of Al alloys: mechanisms determining as-cast grain size in directional solidification, Acta Mater. 53 (2005) 4643–4653.
[17] D. Shu, B. Sun, J. Mi, P.S. Grant, A quantitative study of solute diffusion field effects on heterogeneous nucleation and the grain size of alloys, Acta Mater. 59 (2011) 2135–2144.
[18] Q. Du, Y. Li, An extension of the Kampmann–Wagner numerical model towards as-cast grain size prediction of multicomponent aluminum alloys, Acta Mater. 71 (2014) 380–389.
[19] M.A. Easton, D.H. StJohn, A model of grain refinement incorporating alloy constitution and potency of heterogeneous nucleant particles, Acta Mater. 49 (2001) 1867–1878.
[20] M. Qian, P. Cao, M.A. Easton, S.D. McDonald, D.H. StJohn, An analytical model for constitutional supercooling-driven grain formation and grain size prediction, Acta Mater. 58 (2010) 3262–3270.
[21] H. Men, Z. Fan, Effects of solute content on grain refinement in an isothermal melt, Acta Mater. 59 (2011) 2704–2712.
[22] D.H. StJohn, M. Qian, M.A. Easton, P. Cao, The Interdependence Theory: the relationship between grain formation and nucleant selection, Acta Mater. 59 (2011) 4907–4921.
[23] X.B. Qi, Y. Chen, X.H. Kang, D.Z. Li, Q. Du, An analytical approach for predicting as-cast grain size of inoculated aluminum alloys, Acta Mater. 99 (2015) 337–346.
[24] G. Chai, L. Backerud, L. Arnberg, Relation between grain size and coherency parameters in aluminium alloys, Mater. Sci. Technol. 11 (1995) 1099–1103.
[25] M. Abdel-Reihim, N. Hess, W. Reif, M.E.J. Birch, Effect of solute content on the grain refinement of binary alloys, J. Mater. Sci. 22 (1987) 213–218.
[26] P.A. Tondel, Grain refinement of hypoeutectic aluminum-silicon foundry alloys, in: Norwegian Institute of Technology, Trondheim, Norway, 1994.
[27] P. Hoefs, W. Reif, W. Schneider, Kornfeinung von Aluminium-Gußlegierungen (Grain-refinement of aluminum foundry alloys), Giesserei 81 (1994) 398–406.
[28] L. Baeckerud, M. Johnsson, The relative importance of nucleation and growth mechanisms to control grain size in various aluminum alloys, in: Annual Meeting and Exhibition of the Minerals, Metals and Materials Society (TMS), Anaheim, CA (United States), 1996, pp. 679–685.
[29] J.A. Spittle, J.M. Keeble, M. Al Meshhedani, The grain refinement of Al-Si foundry alloys, in: R. Huglen (Ed.), Light Metals, 1997, pp. 795–800.
[30] J.E.C. Hutt, D.H. Stjohn, L. Hogan, A.K. Dahle, Equiaxed solidification of Al-Si alloys, Mater. Sci. Technol. 15 (1999) 495–500.
[31] Y.C. Lee, A.K. Dahle, D.H. Stjohn, J.E.C. Hutt, The effect of grain refinement and silicon content on grain formation in hypoeutectic Al-Si alloys, Mater. Sci. Eng. A 259 (1999) 43–52.
[32] Y. Birol, Effect of silicon content in grain refining hypoeutectic Al-Si foundry alloys with boron and titanium additions, Mater. Sci. Technol. 28 (2012) 385–389.
[33] H.T. Wu, L.C. Wang, S.K. Kung, Influence of grain refine master alloys addition on A 356 aluminum alloy, J Chin. Foundryman's Assoc. 29 (1981) 18.
[34] G.K. Sigworth, M.M. Guzowski, Gain refining of hypoeutectic Al-Si alloys, AFS Trans. 93 (1985) 907–912.
[35] P.A. Tondel, G. Halvorsen, L. Arnberg, Grain-refinement of hypoeutectic Al-Si foundry alloys by addition of boron containing silicon metal, Miner. Metals Mater. Soc. Warrendale PA (1993) 783–790.
[36] T. Wang, Z. Chen, H. Fu, J. Xu, Y. Fu, T. Li, Grain refining potency of Al-B master alloy on pure aluminum, Scr. Mater. 64 (2011) 1121–1124.
[37] J.A. Marcantonio, L.F. Mondolfo, The nucleation of aluminium by several intermetallic compounds, J. Inst. Metals 98 (1970) 23–27.
[38] S.A. Kori, B.S. Murty, M. Chakraborty, Development of an efficient grain refiner for Al-7Si alloy and its modification with strontium, Mater. Sci. Eng. A 283 (2000) 94–104.
[39] Y. Birol, Grain refinement of pure aluminium and Al-7Si with Al-3B master alloy, Mater. Sci. Technol. 28 (2012) 363–367.
[40] A. Cibula, The mechanism of grain refinement of sand casting in aluminum alloys, J. Inst. Metals 76 (1949-1950) 321–360.
[41] A. Cibula, The grain refinement of aluminum alloys casting by addition of titanium and boron, J. Inst. Metals 80 (1951) 1–16.
[42] P.S. Mohanty, J.E. Gruzleski, Mechanism of grain refinement in aluminium, Acta Metall. Mater. 43 (1995) 2001–2012.
[43] P. Schumacher, A.L. Greer, J. Worth, P.V. Evans, M.A. Kearns, P. Fisher, A.H. Green, New studies of nucleation mechanisms in aluminium alloys: implications for grain refinement practice, Mater. Sci. Technol. 14 (1998) 394–404.
[44] Y. Han, Y. Dai, D. Shu, J. Wang, B. Sun, First-principles calculations on the stability of Al/TiB2 interface, Appl. Phys. Lett. 89 (2006) 144107.
[45] J. Wang, A. Horsfield, U. Schwingenschlögl, P.D. Lee, Heterogeneous nucleation of solid Al from the melt byTiB2andAl3Ti: anab initiomolecular dynamics study, Phys. Rev. B 82 (2010).
[46] T. Qin, Z. Fan, Reconstruction of 2D Al 3 Ti on TiB 2 in an aluminium melt, IOP conference series, Mater. Sci. Eng. 27 (2012) 012004.
[47] J. Nie, H. Ding, Y. Wu, X. Liu, Fabrication of titanium diboride-carbon core-shell structure particles and their application as high-efficiency grain refiners of wrought aluminum alloys, Scr. Mater. 68 (2013) 789–792.
[48] N. Iqbal, N.H. van Dijk, S.E. Offerman, M.P. Moret, L. Katgerman, G.J. Kearley, Real-time observation of grain nucleation and growth during solidification of aluminium alloys, Acta Mater. 53 (2005) 2875–2880.
[49] N. Iqbal, N.H. van Dijk, S.E. Offerman, N. Geerlofs, M.P. Moret, L. Katgerman, G.J. Kearley, In situ investigation of the crystallization kinetics and the mechanism of grain refinement in aluminum alloys, Mater. Sci. Eng. A 416 (2006) 18–32.
[50] P.S. Mohanty, J.E. Gruzvolski, Grain refinement mechanisms of hypoeutectic Al-Si alloys, Acta Metall. Mater. 44 (1996) 3749–3760.
[51] M.-X. Zhang, P.M. Kelly, Crystallographic features of phase transformations in solids, Prog. Mater. Sci. 54 (2009) 1101–1170.
[52] ge-to-edge matching and its applications Part I. Application to the simple HCP/BCC system, in: M.X. Zhang, P.M. Kelly (Eds.), Acta Mater. 53 (2005) 1073–1084.
[53] M.X. Zhang, P.M. Kelly, Edge-to-edge matching and its applications Part II. Application to Mg–Al, Mg–Y and Mg–Mn alloys, Acta Mater. 53 (2005) 1085–1096.
[54] M. Zhang, P. Kelly, M. Easton, J. Taylor, Crystallographic study of grain refinement in aluminum alloys using the edge-to-edge matching model, Acta Mater. 53 (2005) 1427–1438.
[55] M.X. Zhang, P.M. Kelly, M. Qian, J.A. Taylor, Crystallography of grain refinement in Mg–Al based alloys, Acta Mater. 53 (2005) 3261–3270.
[56] Y. Birol, An improved halide salt process to produce Al-B master alloys, Mater. Sci. Technol. 27 (2011) 1846–1850.
[57] Z. Chen, T. Wang, L. Gao, H. Fu, T. Li, Grain refinement and tensile properties improvement of aluminum foundry alloys by inoculation with Al–B master alloy, Mater. Sci. Eng. A 553 (2012) 32–36.
[58] Y. Birol, AlB3 master alloy to grain refine AlSi10Mg and AlSi12Cu aluminium foundry alloys, J. Alloys Compd. 513 (2012) 150–153.
[59] Y. Birol, Performance of AlTi5B1, AlTi3B3 and AlB3 master alloys in refining grain structure of aluminium foundry alloys, Mater. Sci. Technol. 28 (2012) 481–486.
[60] D. Qiu, M.-X. Zhang, P.M. Kelly, Crystallography of heterogeneous nucleation of Mg grains on Al2Y nucleation particles in an Mg–10wt.% Y alloy, Scr. Mater. 61 (2009) 312–315.
[61] G.K. Sigworth, The grain refining of aluminum and phase-relationships in the Al-Ti-B system, Metall. Trans. Phys. Metall. Mater. Sci. 15 (1984) 277–282.
[62] G.S. Vinod Kumar, B.S. Murty, M. Chakraborty, Settling behaviour of TiAl3, TiB2, TiC and AlB2 particles in liquid Al during grain refinement, Int. J. Cast

Metals Res. 23 (2010) 193–204.
[63] V. Raghavan, Al-B-Si (Aluminum-Boron-Silicon), J. Phase Equilib. Diff. 29 (2007) 44–45.
[64] R.W. Olesinski, G.J. Abbaschian, The B–Si (Boron-Silicon) system, Bull. Alloy Phase Diagr.rams 5 (1984) 478–484.
[65] D. Qiu, J.A. Taylor, M.X. Zhang, P.M. Kelly, A mechanism for the poisoning effect of silicon on the grain refinement of Al–Si alloys, Acta Mater. 55 (2007) 1447–1456.